Supplemental Material

A) Total internal reflection imaging

To capture the dynamics of the bubbles at the container (bottle) surface, we employed total internal reflection (TIR) imaging. The geometry of illumination and imaging setup shown in Figure 1 of the main article was configured such that the light underwent total internal reflection, efficiently rejecting out-of-focus light. An example of the difference this makes is shown in Figure S1. We focused our analysis on a region that was approximately 1 cm above the liquid meniscus before the foam was produced in the bottle, consistently for all 4 trials of 5 different salinities. In this region, the bubbles were least affected by the unstable foam collapses for 20,000 s, while the foam height was reduced substantially in the time-regimes I and II, as shown in Figure 4(left) of the main article.

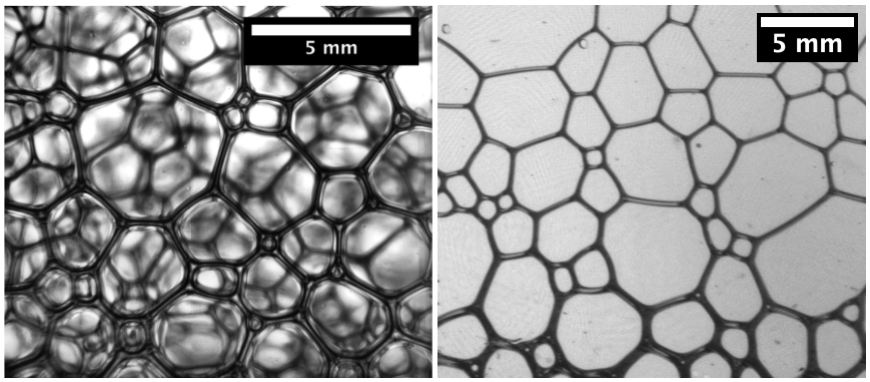

Figure S1: Left: An image obtained using a transmission geometry imaging setup for a bubble-scale imaging. Right: An improved container surface bubble image obtained using total internal reflection for image processing.

B) Liquid level at short times

Figure S2 (top) shows the mean liquid level of all salinities from 0 s up to 500 s. The rapid increase in liquid level is seen between 0 and 420 s, above which shows much smaller changes over time. Using the initial mean liquid level ($\langle$L(t = 0 s)$\rangle$) for all salinities, the initial mean liquid fraction ($\langle\phi(t = 0s)\rangle$) can be estimated as follows:

$$\langle\phi(t=0s)\rangle \approx \frac{\langle L(t=\infty)\rangle - \langle L(t=0s)\rangle}{\langle T(t=0s)\rangle - \langle L(t=0s)\rangle} = \frac{\langle L(t=\infty)\rangle - \langle L(t=0s)\rangle}{\langle F(t=0s)\rangle}, \quad (1)$$

where $\langle$L(t=∞)$\rangle$ is 23.0$\pm$0.5 mm. The values of $\langle$L(t = 0 s)$\rangle$ and $\langle$T(t = 0 s)$\rangle$ are obtained from the data in Figure 3 (right) of the main article. The

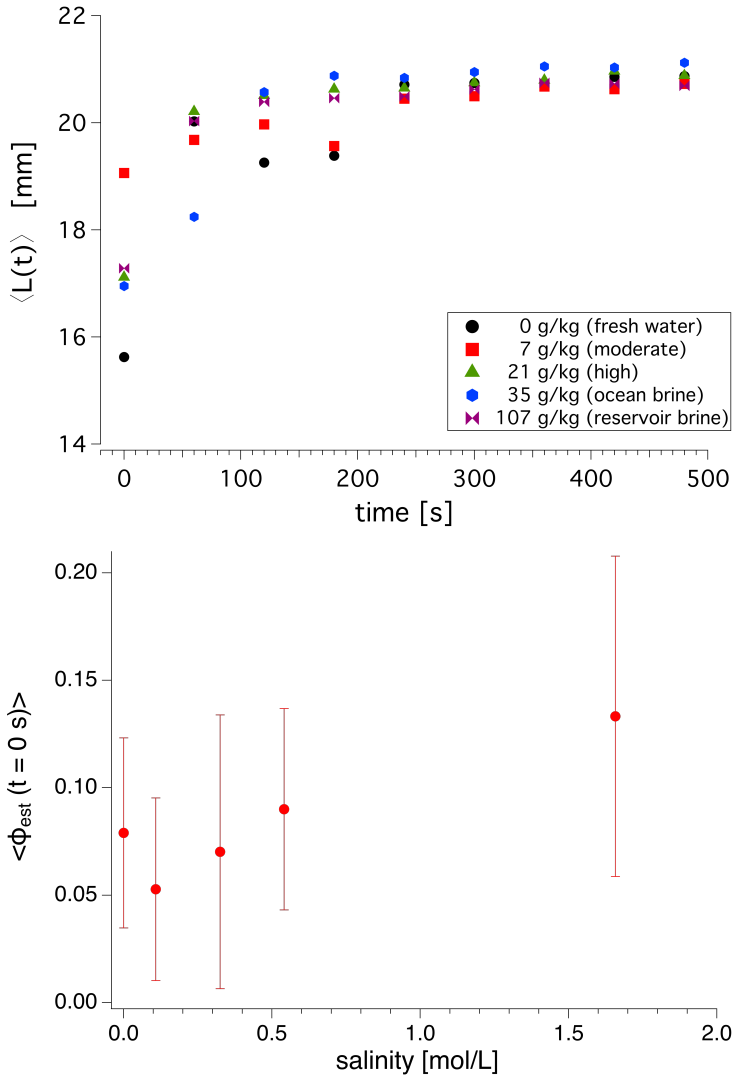

Figure S2: Top: The first 500 s of the mean liquid level is plotted with time for each salinity. (N = 4 trials). The time evolution of the mean liquid level is shown up to 90,000 s (25 hrs) in Figure 3(left) of the main article. Bottom: The effect of salinity on the initial mean liquid fraction of the foam is shown for all salinities. An estimated initial mean liquid fraction ($\langle\phi_{est}$(t = 0 s)$\rangle$) for each salinity is obtained with the measurements of $\langle$L(t)$\rangle$ at t = 0 s. The error bars on $\langle\phi_{est}$(t = 0 s)$\rangle$ are computed using the errors of $\langle$L(t = 0 s)$\rangle$ and $\langle$T(t = 0 s)$\rangle$.

initial mean liquid fraction is plotted as a function of salinity in Figure S2 (bottom).

C) Image perspective corrections

Original bubble images (e.g., Figure S3 left) were corrected for perspective distortion using TransformJ, an ImageJ/FIJI suite for geometrical image transformation[1] (e.g., Figure S3 middle). A transformation matrix was determined for each test with two metric rulers attached to the bottle horizontally (below) and vertically (next to the region of interest), and applied to each image for a pixel-to-metric conversion. The images were then binarized (e.g., Figure S3 right) to obtain the size of each bubble in the region of interest (ROI). Incomplete bubbles at the edges were not included for analysis.

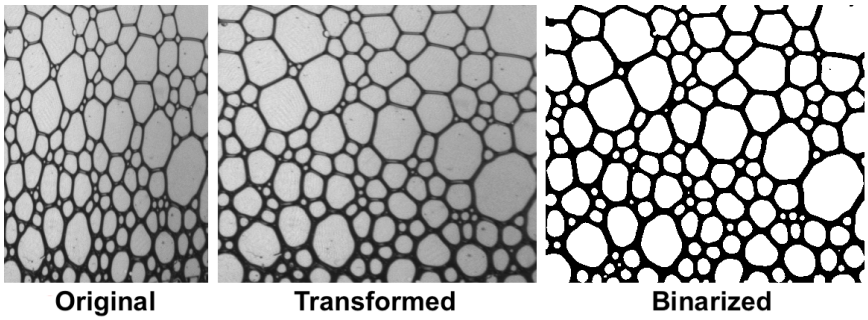

Figure S3: Left: A sample original image of the ROI. Middle: a transformed image of the sample original image. Right: a binarized image of the sample original image for all the bubble-scale measurements.

D) Four replicates: time evolution of cross-sectional mean bubble area at different salinities

In Figure S4 and Figure S5, time-evolution plots of the cross-sectional mean bubble area $\langle A(t) \rangle$ and the corresponding bubble count used to compute the $\langle A(t) \rangle$ in the full ROI are shown for all 4 trials of each salinity.

[1] https://imagescience.org/meijering/software/transformj/

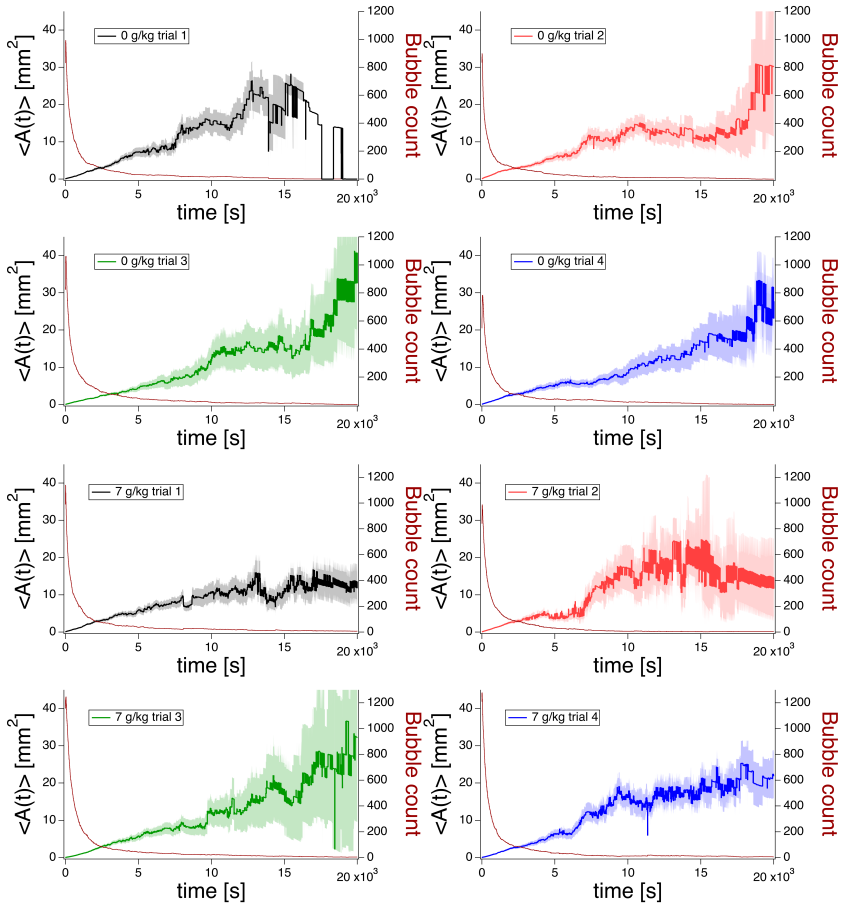

Figure S4: The time evolution of the mean cross-sectional area of bubbles and corresponding bubble counts (shown in darker red) are plotted for each individual trial at 0 g/kg (shown in the top four panels) and 7 g/kg (shown in the bottom four panels). These bubble-scale measurements were acquired from the full region of interest near the bottom of the foam for each trial. The error bars on the mean bubble area measurements represent the standard deviation of the mean.

In Figure S6, the initial mean bubble area $\langle A_0 \rangle$(top panel) and the mean bubble area $\langle A(t) \rangle$ at selected times (bottom panel) are plotted against the salinity. Among the five different salinities $\langle A_0 \rangle$ is not significantly different. However, for the highest salinity, $\langle A(t) \rangle$ is clearly the smallest at 9000 s and again at later times of 18,000 s and 19,998 s.

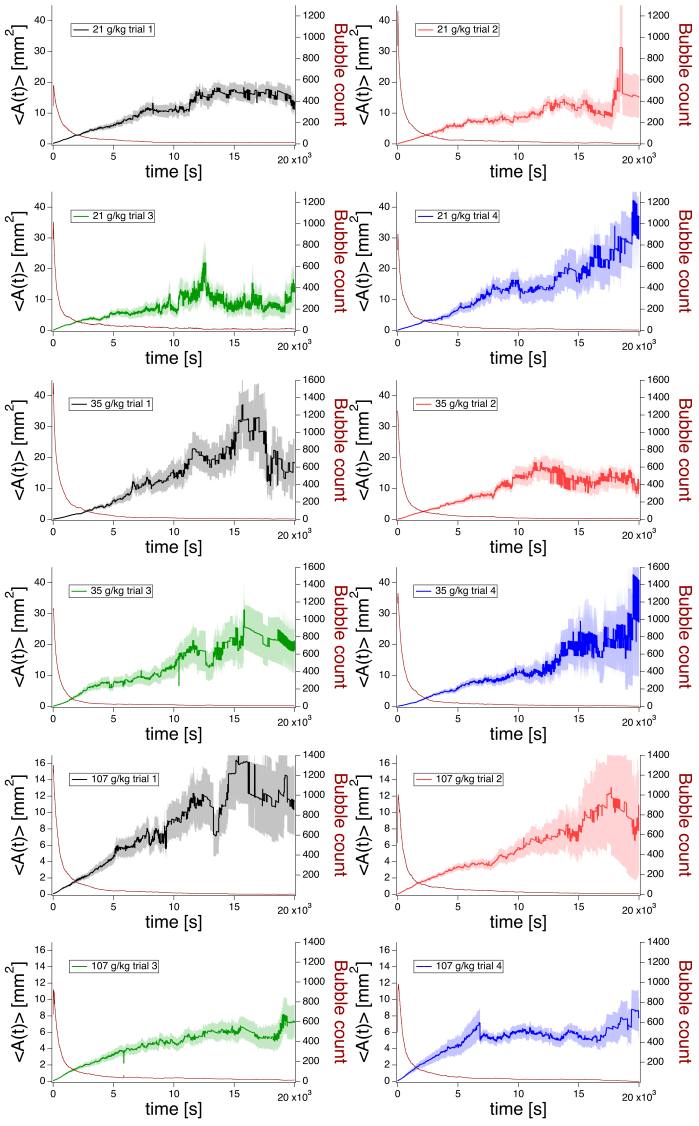

Figure S5: The time evolution of the mean cross-sectional area of bubbles and corresponding bubble counts (shown in darker red) are plotted for each individual trial at 21 g/kg (shown in the top four panels), 35 g/kg (shown in the middle four panels) and 107 g/kg (shown in the bottom four panels). These bubble-scale measurements were acquired from the full region of interest near the bottom of the foam for each trial. The error bars on the mean bubble area measurements represent the standard deviation of the mean.

E) Evolution of macroscopic foam height (regime III) and cross-sectional mean bubble area

Figure S7 shows the time-evolution of the mean macroscopic foam height $\langle F(t) \rangle$ in regime III (left column) and the corresponding $\langle A(t) \rangle$ (right col-

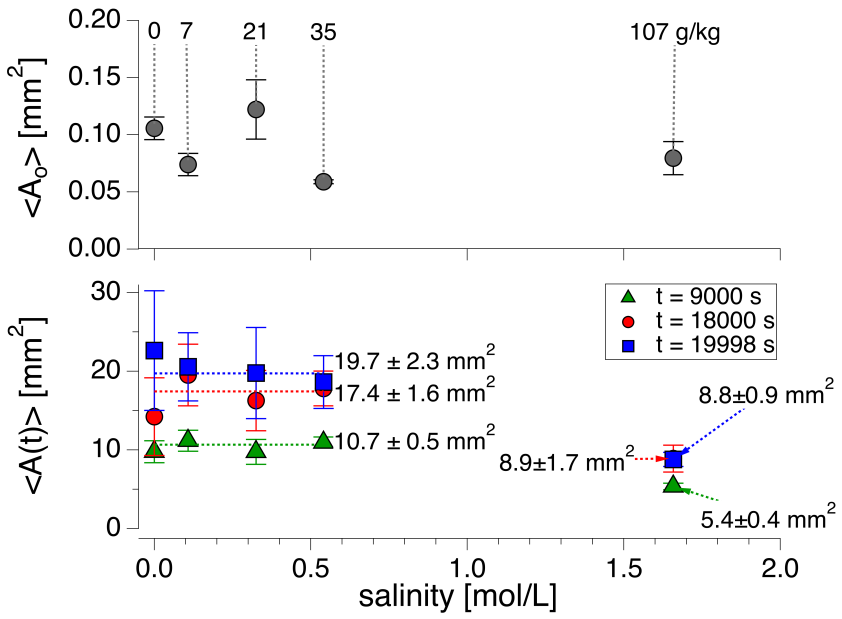

Figure S6: **Comparison of mean bubble cross-sectional area $\langle A(t)\rangle$ for different times**: Top: The initial mean cross-sectional area $\langle A_0\rangle$ of bubbles in the full region shows little dependence on salinity, within errors. Bottom: $\langle A(t)\rangle$ for three additional times, 9000 s, 18,000 s and 19,998 s, are not significantly dependent on salinity, except for the highest salinity (1.7 mol/L).

umn) for all salinities. Each plot shows the fit obtained for determining the J_{mean} or K_{mean}, as shown in Figures 5(left) and 8(right) of the main article, respectively.

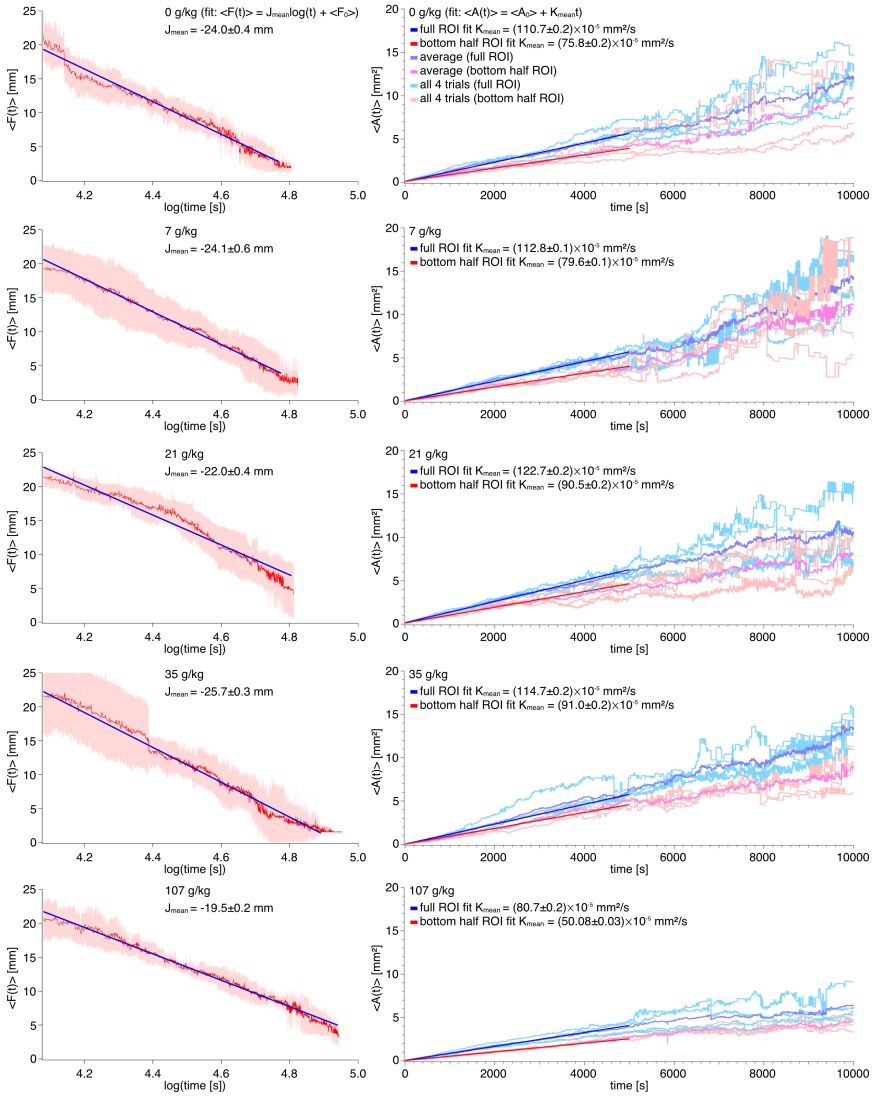

Figure S7: Comparing the macroscopic foam and the bubble scale dynamics: Time evolution of the mean foam height $\langle F(t) \rangle$ in time regime III (left column) and the cross-sectional mean bubble area $\langle A(t) \rangle$ (right column) of the 5 different salinities (top to bottom: 0 g/kg, 7 g/kg, 21 g/kg, 35 g/kg, 107 g/kg) are plotted, and the fit to a linear dependence is shown for each salinity. Left: In the $\langle F(t) \rangle$ plots, the red data symbols represent the average of the individual trials datasets: the data in time regime III is fit to a linear function. The pink scatter represents the standard error of the mean from the 4 individual trials for each salinity. Right: In each of the $\langle A(t) \rangle$ plots, the purple data represent the average $\langle A(t) \rangle$ over all trials of a given salinity (shown in light blue) for the full region of interest (ROI). This was fitted (in blue) with a linear function as shown in the figure legend. Similarly, the dark pink traces represent $\langle A(t) \rangle$ of all trials of a salinity (shown in light pink) for the bottom half of the ROI. This was fitted (in red) with a linear function as shown in the figure legend over the same first 5000 s.

F) Foaming liquid properties

Surface tension, viscosity and density of the foaming solutions were measured using an interfacial tension meter (IFT 700, Vinci Technologies), a rheometer (MCR-301, Anton Paar), and a hand-held densitometer (DMA-35, Anton Paar), respectively, for all foaming solutions used in the study. Figure S8 shows the surface tension of the foaming solutions. There is little change in the surface tension with increasing salinity, and one can use an average value of $\gamma = 31.6 \pm 0.2$ mN/m.

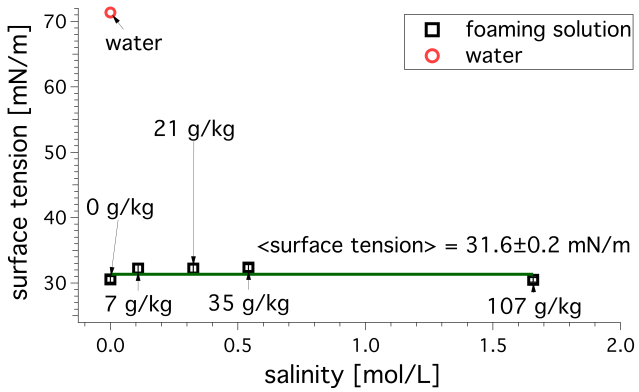

Figure S8: Surface tension of the solutions is plotted against salinity. The red circle marker represents the surface tension of deionized water. The error bars exist within the data point markers. N > 10 trials for all foaming solutions. Sample: 0.0047 ± 0.0002 mol/L of Triton X-100 surfactant in various brine concentrations.

A key parameter in foam stability is the kinetic coefficient M that goes into the von Neumann for bubble coarsening. This parameter clearly depends on the viscosity of the foaming solution, which is plotted as a function of salinity in Figure S9. Of all the liquid properties, the viscosity is seen to increase the most, by more than 20% from 0 g/kg to 107 g/kg brine concentrations.

Figure S10 shows the density of the foaming solutions. This is seen to increase linearly with salinity, as expected, from ∼1 g/mL for the foaming solution with no salt to 1.07 g/mL at the highest salinity. The density obtained for distilled water is shown (circle marker in red) as a reference.

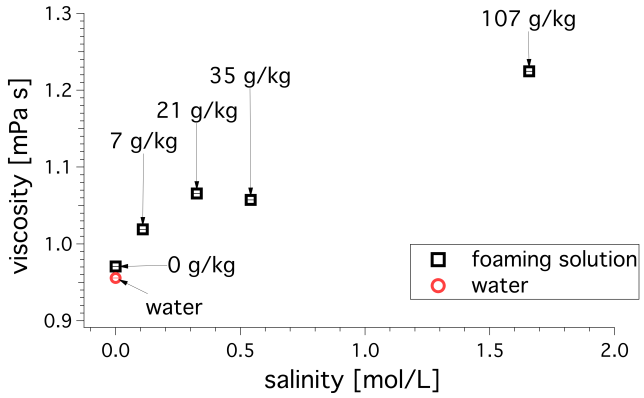

Figure S9: Viscosity of the solutions is plotted against salinity. The red circle marker represents the viscosity of deionized water. Sample: 0.0047 ± 0.0002 mol/L of Triton X-100 surfactant in various brine concentrations.

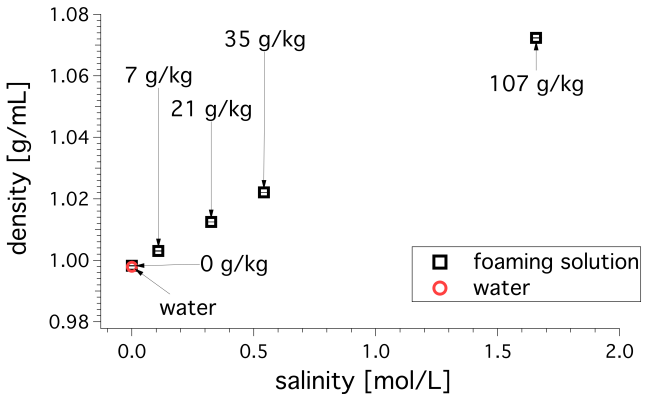

Figure S10: Density of the solutions is plotted against salinity. The red circle marker represents the density of deionized water, which was measured in between each sample measurement and resulted in a consistent value of 0.9979 g/mL every time at a constant temperature $T = 21.2° \pm 0.1°$. We ensured no frequency-specific density change due to contamination or existence of bubbles in solutions. The error bars exist within the data point markers. N = 3 trials. Sample: 0.0047 ± 0.0002 mol/L of Triton X-100 surfactant in various brine concentrations.